

This work was written as part of one of the author's official duties as an Employee of the United States Government and is therefore a work of the United States Government. In accordance with 17 U.S.C. 105, no copyright protection is available for such works under U.S. Law.

Public Domain Mark 1.0

<https://creativecommons.org/publicdomain/mark/1.0/>

Access to this work was provided by the University of Maryland, Baltimore County (UMBC) ScholarWorks@UMBC digital repository on the Maryland Shared Open Access (MD-SOAR) platform.

Please provide feedback

Please support the ScholarWorks@UMBC repository by emailing scholarworks-group@umbc.edu and telling us what having access to this work means to you and why it's important to you. Thank you.

The Role of Convection in Tropical Ozone Trends (1998-2018) Based on SHADOZ Profiles

Anne M. Thompson¹, Ryan Michael Stauffer², Jacquelyn Cecile Witte³, Debra E Kollonige⁴, Jerald R. Ziemke², and Krzysztof Wargan⁵

¹NASA-GODDARD

²NASA Goddard Space Flight Center

³National Center for Atmospheric Research

⁴Unknown

⁵SSAI at NASA Goddard Space Flight Center

November 24, 2022

Abstract

Quantifying variability in the lowermost stratosphere (LMS) is important because of feedbacks among changing temperature, dynamics and species like ozone. We used reprocessed Southern Hemisphere Additional Ozonesondes data from 1998-2018 in a Multiple Linear Regression (MLR) model to analyze variability and trends in free tropospheric (FT) and LMS ozone across five well-distributed tropical regions. The MLR also computed trends in a proxy for convection as determined from laminae in each ozonesonde-radiosonde pair. Only the equatorial Americas exhibits statistically significant annual trends in FT or LMS ozone. At the other sites, ozonetrends occur in isolated layers during months when convection has changed, February-April or July-November. Our results imply that large FT ozone increases reported for populated tropical areas may be caused by growing pollution overlying smaller changes caused by perturbed dynamics. They also provide regional data for evaluating LMS ozonetrends based on zonal averages of often sparse satellite measurements

The Role of Convection in Tropical Ozone Trends (1998-2018) Based on SHADOZ Profiles

12 June 2020

Anne M. Thompson^{1*}, Ryan M. Stauffer^{1,2}, Jacquelyn C. Witte³, Debra E. Kollonige^{2,4}, Krzysztof Wargan^{1,4}, Jerry R. Ziemke^{1,5}

¹NASA/Goddard Space Flight Center (GSFC), Greenbelt, MD, USA
anne.m.thompson@nasa.gov; ORCID: 0000-0002-7829-0920

²Earth System Science Interdisciplinary Center, University of Maryland, College Park, MD, USA
ryan.m.stauffer@nasa.gov; ORCID: 0000-0002-8583-7795

³National Center for Atmospheric Research Earth Observations Laboratory, Boulder, CO, USA
jwitte@ucar.edu; ORCID: 0000-0002-4110-5277

⁴Science Systems and Applications, Inc., Lanham, MD, USA
debra.e.kollonige@nasa.gov; ORCID: 0000-0002-6597-328X; krzysztof.wargan-1@nasa.gov; ORCID: 0000-0002-3795-2983

⁵Morgan State University, Baltimore, Maryland, USA
gerald.r.ziemke@nasa.gov; ORCID: 0000-0002-5575-3654

*Corresponding author: Anne M. Thompson (anne.m.thompson@nasa.gov)

Key Points:

- Trends (1998-2018) in free tropospheric (FT) and lowermost stratospheric (LMS) ozone and a convective proxy at SHADOZ sites were computed
- One station displayed an annual FT ozone trend (~5%/dec) and LMS loss (-3%/dec). Ozone changed only in certain months at four other sites
- LMS ozone increases (decreases) occur in the low (high)-ozone months; these may tend to counteract one another

Keywords: Tropical Ozone Trends, Lower Stratosphere, Ozonesondes, Free Troposphere, SHADOZ

Index Terms: 345, 365, 1620, 3309, 3314

Abstract

Quantifying variability in the lowermost stratosphere (LMS) is important because of feedbacks among changing temperature, dynamics and species like ozone. We used reprocessed Southern Hemisphere Additional Ozonesondes data from 1998-2018 in a Multiple Linear Regression (MLR) model to analyze variability and trends in free tropospheric (FT) and LMS ozone across five well-distributed tropical regions. The MLR also computed trends in a proxy for convection as determined from laminae in each ozonesonde-radiosonde pair. Only the equatorial Americas exhibits statistically significant annual trends in FT or LMS ozone. At the other sites, ozone trends occur in isolated layers during months when convection has changed, February-April or July-November. Our results imply that large FT ozone increases reported for populated tropical areas may be caused by growing pollution overlying smaller changes caused by perturbed dynamics. They also provide regional data for evaluating LMS ozone trends based on zonal averages of often sparse satellite measurements.

Plain Language Summary

Understanding variability in lowermost stratosphere (LMS) ozone is an important topic in the climate assessment community because of feedbacks among changing temperature, dynamics and species like ozone. Most LMS evaluations are based on satellite observations. Tropospheric ozone assessments rely heavily on profiles from commercial aircraft. Ozonesonde measurements constitute an independent dataset that encompasses both LMS and troposphere. We used v06 Southern Hemisphere Additional Ozonesondes data from 1998-2018 in a Multiple Linear Regression model to analyze variability and trends in free tropospheric (FT) and LMS ozone across five well-distributed tropical sites. Our findings: (1) Only one SHADOZ site, in the equatorial Americas, exhibits small positive FT and negative LMS ozone trends on an annually averaged basis. (2) At the other 4 sites, trends only occur in isolated layers during months with decreasing (February-April) or increasing (July-September) convection. (3) The latter ozone changes are always positive in the FT. Because most SHADOZ stations are very remote, the results do not suggest large-scale tropical FT O₃ increases. They do imply that in the urban tropics where rising emissions create additional ozone, the trends observed in aircraft profiles may overlie smaller FT ozone increases caused by perturbed dynamics.

1 Introduction

Ozonesonde data are widely used by the scientific community for satellite validation, model evaluation and analysis of trends, especially in the free troposphere (FT) through lowermost stratosphere (LMS), i.e., from ~5-20 km, where uncertainties in most satellite measurements are relatively large (*SPARC/IozoneC/GAW*, 2019). Many studies have used data from SHADOZ (Southern Hemisphere Additional Ozonesondes; *Thompson et al.*, 2003; 2012), a 14-station tropical network with > 8300 profiles since 1998, to investigate FT and LMS ozone variability, layers in which there are critical feedbacks among temperature, dynamics and species like water vapor and ozone.

1.1 Variability in FT and LMS Ozone: Role of Convection

Early studies of FT and LMS ozone variability with SHADOZ profiles focused on convective influences (*Folkins et al.*, 2002) and biomass burning (*Oltmans et al.*, 2001; *Thompson et al.*, 2003). ENSO-perturbed patterns of convection, precipitation and fire induce variability in FT and LMS ozone that vary station to station (*Randel and Thompson*, 2011). *Thompson et al.* (2011) reported significant connections between LMS ozone vertical structure and convectively-generated waves inferred from SHADOZ profiles. Convective links to FT ozone structure are clearly evident when profiles are classified by Self-Organizing Maps (SOM; *Jensen et al.*, 2012; *Stauffer et al.*, 2018).

1.2 Trends in FT and LMS Tropical Ozone. Scope of Present Study

Studies with satellite data, including Aura OMI and MLS ozone, reflect uncertainty in both FT and LMS trends over the past 15-20 years. A review of various FT satellite products displays a range of spatial ozone changes with disagreements in magnitude and sign (*Gaudel et al.*, 2018). Recent work with merged satellite datasets (*SPARC/IO3C/GAW*, 2019) in the mid- to lower stratosphere, along with chemistry transport and assimilation models, indicate the uncertainty of LMS ozone trends (*Ball et al.*, 2018; *Chipperfield et al.*, 2018; *Wargan et al.*, 2018), at least on a zonally averaged basis. We address this situation with ozone profiles over a range of stations using v06 SHADOZ data (*Thompson et al.*, 2017; *Witte et al.*, 2017; 2018) that are better resolved than satellite measurements below 20 km. First, we review seasonal and regional variations in FT and LMS ozone, then quantify their convective activity through analysis of ozone and radiosonde laminae. Second, trends in ozone profiles and convection are

determined with a standard Multiple Linear Regression (MLR) model. Data and analysis methods appear in **Section 2** with Results and Discussion in **Section 3**. **Section 4** is a summary.

2 Data and Methods of Analysis

2.1 Reprocessed SHADOZ Data

Ozone data are taken from the SHADOZ archive (<https://tropo.gsfc.nasa.gov/shadoz>); they originate from electrochemical concentration cell ozonesondes coupled to standard radiosondes. In order to focus on convective impacts in the tropics we use v06 data from eight of the 14 long-term stations (**Table 1**). For more reliable statistics three of the “stations” or “sites” as they are referred to (**Figure 1**), are based on combining profiles from pairs of launch locations abbreviated as SC-Para; Nat-Asc; KL-Java. The v06 data, reprocessed in 2016-2018, reduced inhomogeneities due to instrument or data-handling changes (Witte *et al.*, 2017; 2018) such that sonde total ozone column (TOC) amounts agree with ground-based or satellite data within 2% for all but one station. Data from a number of SHADOZ stations display a 3-6% dropoff in TOC after 2013 (Sterling *et al.*, 2018; Stauffer *et al.*, 2020) relative to satellite and/or ground-based readings. For the stations analyzed here, the dropoff is confined to readings above 50 hPa (~20 km) and does not affect the results.

2.2 Free Tropopause and LMS Definitions

Illustrations in **Section 3** span the surface to 20 km and refer to two FT segments: 5-10 km; 10-15 km. We use 15-20 km for the lowermost stratosphere (LMS), because this is where convective impacts on waves maximize (Thompson *et al.*, 2011) and where Randel *et al.* (2007) identified a distinct ozone annual cycle driven by the Brewer-Dobson circulation. The LMS includes most of the tropical tropopause layer (13.5-18.5 km) and several km above the tropical cold-point and thermal lapse-rate tropopauses over the selected SHADOZ sites (Thompson *et al.*, 2012).

2.3 Multiple Linear Regression Model (MLR)

In order to quantify factors leading to seasonal and interannual variability as well as trends, a standard multiple linear regression model (MLR; original version Stolarski *et al.*, 1991, updated in Ziemke *et al.*, 2019) is applied to monthly mean ozone profiles for the 5 sites: the 3 combined sites, Nairobi, Samoa. The model includes terms for annual and semi-annual cycles

and oscillations prevalent in tropics: QBO, SOI (Southern Oscillation Index) and DMI (Indian Ocean Dipole Moment Index):

$$O_3(t) = A(t) + B(t)t + C(t)SOI(t) + D(t)QBO(t) + E(t)DMI(t) + \varepsilon(t)$$

where t is month. The coefficients are as follows: A is periodic with 12, 6, 4, and 3 month cycles, and B through D have a period of 12 months, where A is the mean seasonal cycle and B represents the month-dependent linear trend. The model includes data from the SOI (<https://www.ncdc.noaa.gov/teleconnections/enso/indicators/soi/>), the u30 QBO index (<https://www.cpc.ncep.noaa.gov/data/indices/qbo.u30.index>), and DMI (<https://stateoftheocean.osmc.noaa.gov/sur/ind/dmi.php>). The $\varepsilon(t)$ is the residual, i.e., the difference between the best-fit model and the raw data. Monthly ozone data and model fits for the mid FT (5-10 km) and LMS (**Figures S1 and S2**) are well-correlated; for the LMS the correlation coefficients r are ~ 0.8 (**Figure S2**).

2.4 Laminar Identification (LID) and GW Indices

The Laminar Identification (LID) method was used to identify convective signatures in ozone profiles for the 1998-2009 SHADOZ data (*Thompson et al.*, 2011). The LID technique, applied here to the 1998-2018 record (**Table 1**), is based on the coherence of laminae in each ozone and potential temperature profile pair; laminae are identified as deviations from running means calculated every 0.5 km from surface to 20 km. When the potential temperature and ozone laminae at a given level are strongly correlated, as often occurs in the LMS, the presence of a convectively-generated gravity wave (GW) is inferred. The GW occurrence is a proxy for a convective event. Convective influence is quantified by the monthly GW frequency (GWF), defined as the percent ratio of profiles exhibiting the GW signal relative to the total number of profiles within a given month. A GW Index (GWI), defined as the fraction of the 15-20 km ozone column (in Dobson Units, DU) that exhibits a GW signature, combines convection and its LMS ozone impact. Monthly mean GWI and the altitude of the 380 K potential temperature surface, often used to mark the tropical tropopause, over 1998-2018 are also ingested in the MLR model.

2.5 Self-Organizing Maps (SOM)

We have used SOM, a machine-learning technique, to classify ozone profiles in terms of meteorological or chemical influences (*Stauffer et al.*, 2016). The entire set of ozone profiles for each station is ingested into the SOM code to obtain initial nodes (i.e., cluster centroids) via a

linear interpolation between the two largest components of the ensemble. Subsequent iterations assign a given profile to its “best match” until a cluster mean is obtained. We adopt key elements of the procedure in *Stauffer et al.* (2018): 1) a four-cluster 2x2 SOM is used to avoid clusters with too few members for meaningful statistics (cf *Jensen et al.*, 2012); 2) SOM clusters are numbered 1 to 4 based on the cluster “mean” ozone profile. The result is a consistent definition of Cluster 1 and Cluster 4 as “low” and “high” ozone for each site, respectively.

3 Results and Discussion

3.1 Seasonal Cycles in Ozone and Convective Influence

Figure 2 displays the 5-site monthly ozone climatology from the surface to 20 km. Regional differences in vertical structure are pronounced. Red to yellow (~90-60 ppbv) colors never appear in mid FT ozone over the equatorial Americas (SC-Para, **Figure 2a**), KL-Java or Samoa (**Figures 2d,e**). Conversely, FT ozone values ≤ 30 ppbv never appear over Nat-Asc or Nairobi (**Figures 2b,c**). These contrasts partly reflect regional differences in ascending vs. descending nodes of the Walker circulation. The mean total ozone column thickness over the south tropical Atlantic Ocean is 5% greater than over the western Pacific, giving rise to the well-known tropospheric zonal wave-one (*Thompson et al.*, 2003). Compared to the FT, there is less regional variability in LMS ozone (Fig. 8 in *Thompson et al.*, 2017) and a large seasonal cycle (**Figure 3c**; cf *Randel et al.*, 2007).

FT ozone seasonality is unique at each site due to the timing of various dynamical and chemical influences. Localized FT ozone maxima occur largely from imported fire pollution: SC-Para in March and after August; at KL-Java in April-May (**Figures 2a,d**); features at 6-8 km over Nat-Asc and Samoa August to November (**Figures 2b,e**); Nairobi (**Figure 2c**) in June and after August. Month-to-month changes viewed as anomalies from annual mean ozone (**Figure 3a,b**) appear complex but they reveal 3-4 distinct transitions when filtered with a criterion of a 5 ppbv gradient (**Figure S3**). The transition times (white vertical lines in **Figure 2**), March-April, June-August, September-November, are similar at all locations. Convective influence, given by GWF (**Figure S4**), with transitions marked as for ozone, shifts during the same periods. GWF reaches 50-70% February-April at all locations (**Figure S4**), during which ozone minima above 8 km, attributed to convective redistribution of near-surface lower ozone air (**Figure 2**), appear over all stations except Nairobi.

3.2 FT and LMS Ozone Changes (1998-2018)

In **Figure 4** FT and LMS changes in ozone mixing ratio (%/decade during 1998-2018) are displayed, based on monthly mean trends computed with the MLR model. Corresponding values in three layers appear in **Table 1**. Shades of red (blue) in **Figure 4** represent ozone increases (decreases); cyan hatching denotes statistical (95%) significance. For four stations (**Figures 4a-d**) there is a similar pattern in February through April with significant ozone trends at various altitudes in the FT and/or LMS. At SC-Para (**Figure 4a**) LMS ozone losses set in after May, extending in some layers to November. Mid-late year LMS ozone losses also occur over the four other sites (**Figures 4b-d**). However, **Table 1** (bold values) shows that these LMS ozone losses are only significant in isolated months. Thus, there is no overall trend except at SC-Para where a mean LMS loss (-3%/decade) overlies a positive annual FT ozone trend of ~5%/decade.

The dominant impact of southern African and South American fires on Nat-Asc and Samoa FT ozone in July through November is well-documented (*Oltmans et al.*, 2001; *Thompson et al.*, 2003). A near-absence of trends over these sites in the second half of the year (**Figures 4b,e**) may signify little change in fires since 1998. FT ozone increases over KL-Java (**Figure 4d**) in February-March may be related to the southeast Asia fire season and/or to growing urban emissions (*Zhang et al.*, 2016).

The annual cycles illustrated in **Figure 3** provide context for the changes shown in **Figure 4** and **Table 1**:

- FT ozone changes (5-15 km) are never significantly negative for any month
- In the mid FT (5-10 km), ozone trends are significantly positive only in the lowest-ozone, convectively active time of year (February to May)
- In the LMS, statistically significant ozone increases occur only during the low-ozone time of year (January to May) and decreases only during the higher-ozone period (June/July through November/December)

Zhang et al. (2016) and *Gaudel et al.* (2018) presented analyses of tropospheric ozone changes at different periods within 1994-2015. In those studies both satellite-derived tropospheric ozone columns and commercial aircraft profiles include boundary-layer ozone so they exceed the FT changes calculated here. The satellite trends, e.g., in *Zhang et al.* (2016; supplement), do not capture the negligibly small FT ozone changes over Nat-Asc and Nairobi.

3.3 Convective Influences in Ozone Trends

Sections 3.1 and 3.2 described an implicit role for convection in the seasonal variability of FT and LMS ozone. Here, we examine links between ozone profile variability and convection using the LID and SOM methods (**Sections 2.4 and 2.5**). The classification of ozone profiles for several SHADOZ sites in a 2x2 SOM (*Stauffer et al.*, 2018) established an anticorrelation between FT ozone mixing ratios and convective activity, where the latter was quantified by meteorological parameters at sonde launch time (Figure 7 in *Stauffer et al.*, 2018). The SOM in **Figure S5** shows similar relationships. The characteristic S-shapes in the upper FT in Cluster 1 (**Figure S5a**) display the lowest mixing ratios whereas much of the elevated ozone in Cluster 4 (**Figure S5b**) derives from imported pollution at 5-10 km. The GWF Cluster 1 (**Figure S5c**), representing maximum convection, is dominated by January-May profiles (not shown), that is, when there are positive FT ozone changes at all sites except Samoa.

We consider whether changes in GWI (the parameter that combines GWF and its impact on LMS ozone) and 380 K altitude trends (**Figure S6**) can explain ozone trends (**Table 1**). Statistically significant negative trends in GWI during January/February and March at Nat-Asc and Nairobi (**Figure 5b,c**) coincide with increasing LMS ozone (**Figure 4b,c**). This combination implies less wave (convective) activity. With suppressed convection, there are positive FT ozone changes in January and February at Nat-Asc and Nairobi (cf **Figures 4b,c**). Samoa (**Figure 5e**) exhibits a January loss in GWI but no significant LMS or FT ozone change.

There are large GWI increases at Nat-Asc (**Figure 5b**) in October and November but no LMS ozone changes, consistent with increasing convection in the latter part of the year. This pattern could also be explained by significant positive trends in the tropopause altitude at Nat-Asc as well as at Nairobi and SC-Para in July to September (**Figure S6a-c**). Increasing convection at KL-Java (**Figure 5d**) is implied by June and July GWI increases coincident with a July LMS ozone loss. There is an insignificant positive 380 K altitude trend (**Figure S6d**).

4 Summary

The 21-year SHADOZ record (1998-2018) of ozone profiles from five well-distributed tropical regions was used to compute trends in the FT (5-15 km) and LMS (15-20 km). Only at one station, SC-Para, is there an annually averaged FT ozone increase, ~5%/decade, or annual LMS ozone loss, -3%/decade. Changes in both FT and LMS ozone vary considerably from site to

site, with four of five stations displaying significant increases during February to April. Using proxies for convection, it appears that these FT ozone increases may be due to reduced vertical mixing. LMS ozone losses later in the year may take place when convective influence and the tropopause altitude are both increasing.

Randel et al. (2007) and *Stolarski et al.* (2014) used satellite observations and meteorological analyses to describe multiple dynamical influences on LMS ozone. Our simplified study interprets FT and LMS ozone changes with reference to a single proxy for vertical motion that is inferred from the sounding data. Nonetheless, the relatively small, geographically distinct changes provide a reference for evaluating ozone trends derived from satellite products that are typically presented as zonal averages (*Ball et al.*, 2018). Model interpretations of our results are required to assess whether recent reports of large tropical ozone increases (*Zhang et al.*, 2016; *Gaudel et al.*, 2018) might reflect growing urban emissions superimposed on smaller trends due to changes in dynamics. Model diagnostics are also required to evaluate the contributions of diverse dynamical processes to ozone changes in the LMS.

Acknowledgments

Support is gratefully acknowledged from the NASA Upper Air Research Program (K. W. Jucks, Program Manager), S-NPP and JPSS (J. F. Gleason, Project Scientist) and the NASA Post-doctoral Program to RMS. We are grateful to O. R. Cooper (CIRES/NOAA-CSL) and W. Randel (NCAR) for helpful comments. SHADOZ v06 profile data are available at <https://tropo.gsfc.nasa.gov/shadoz/Archive.html>.

References

- Ball, W. T., Alsing, J., Mortlock, D. J., Staehelin, J., Haigh, J. D., Peter, T., et al. (2018). Continuous decline in lower stratospheric ozone off sets ozone layer recovery, *Atmos. Chem. Phys.*, 18, 1379–1394, <https://doi.org/10.5194/acp-18-1379-2018>
- Chipperfield, M. P., Dhomse, S., Hossaini, R., Feng, W., Santee, M. L., Weber, M., et al. (2018). On the cause of recent variations in lower stratospheric ozone, *Geophys. Res. Lett.*, 45, <https://doi.org/10.1029/2018GL078071>.
- Folkins, I. Braun, C., Thompson, A. M., Witte, J. C. (2002). Tropical ozone as in indicator of deep convective outflow, *J. Geophys. Res.*, 107, D13, doi: 10.1029/2001JD001178.

- Gaudel, A., Cooper, O. R., Ancellet, G., Barret, B., Boynard, A., Burrows, J. P., et al. (2018). Tropospheric Ozone Assessment Report: Present-day distribution and trends of tropospheric ozone relevant to climate and global atmospheric chemistry model evaluation, *Elem. Sci. Anth.*, 6: 39, doi: <https://doi.org/10.1525/elementa.291>.
- Jensen, A. A., Thompson, A. M., Schmidlin, F. J. (2012). Classification of Ascension Island and Natal ozonesondes using self-organizing maps, *J. Geophys. Res.*, 117, D04302, doi:10.1029/2011JD016573.
- Oltmans, S. J., Johnson, B. J., Harris, J. M., Vömel, H., Thompson, A. M., et al. (2001). Ozone in the Pacific tropical troposphere from ozonesonde observations, *J. Geophys. Res.*, 106, 32503-32526, doi: <https://doi.org/10.1029/2000JD900834>.
- Randel, W. J., M. Park, and F. Wu (2007). A large annual cycle in ozone above the tropical tropopause linked to the Brewer–Dobson circulation, *J. Atmos. Sci.*, 64, 4479-4488, doi: 10.1175/2007JAS2409.1.
- Randel, W. J., and A. M. Thompson (2011), Interannual variability and trends in tropical ozone derived from SHADOZ ozonesondes and SAGE II satellite data, *J. Geophys. Res.*, 116, D07303, doi:10.1029/2010JD015195.
- SPARC/IO3C/GAW (2019). SPARC/IO3C/GAW Report on Long-term Ozone Trends and Uncertainties in the Stratosphere, I. Petropavlovskikh, S. Godin-Beekmann, D. Hubert, R. Damadeo, B. Hassler, V. Sofieva (Eds.), SPARC Report No. 9, GAW Report No. 241, WCRP-17/2018, doi: 10.17874/f899e57a20b; www.sparc-climate.org/publications/sparc-reports.
- Stauffer, R. M., Thompson, A. M., Witte, J. C. (2018). Characterizing global ozonesonde profile variability from surface to the UT/LS with a clustering technique and MERRA-2 reanalysis, *J. Geophys. Res. Atmos.*, 123, 6213–6229, <https://doi.org/10.1029/2018JD028465>.
- Stauffer, R. M., Thompson, A. M., Kollonige, D. E., Witte, J. C., Tarasick, D. W., Davies, J., et al. (2020). A post-2013 dropoff in total ozone at a third of global ozonesonde stations: Electrochemical concentration cell instrument artifacts? *Geophys. Res. Lett.*, 47, e2019GL086791. <https://doi.org/10.1029/2019GL086791>.
- Sterling, C. W., Johnson, B. J., Oltmans, S. J., Smit, H. G. J., Jordan, A. F., Cullis, P. D., et al. (2018). Homogenizing and estimating the uncertainty in NOAA's long-term vertical ozone profile records measured with the electrochemical concentration cell ozonesonde, *Atmos. Meas. Tech.*, 11, 3661-3687, <https://doi.org/10.5194/amt-11-3661-2018>.

Stolarski, R. S., Bloomfield, P. R., McPeters, R. D., Herman, J. R. (1991). Total ozone trends deduced from Nimbus 7 TOMS data, *Geophys. Res. Lett.*, 18, 1015-1018, <https://doi.org/10.1029/91GL01302>.

Stolarski, R. S., Waugh, D. W., Wang, L., Oman, L. D., Douglass, A. R., Newman, P. A. (2014). Seasonal variation of ozone in the tropical lower stratosphere: Southern tropics are different from northern tropics, *J. Geophys. Res. Atmos.*, 119, 6196–6206, doi:10.1002/2013JD021294.

Thompson, A. M., Witte, J. C., Oltmans, S. J., Schmidlin, F. J., Logan, J. A., et al. (2003). Southern Hemisphere ADditional Ozonesondes (SHADOZ) 1998-2000 tropical ozone climatology. 2. Tropospheric Variability and the zonal wave-one, *J. Geophys. Res. Atmos.*, 108, 8241, doi: <https://doi.org/10.1029/2002JD002241>.

Thompson, A. M., Allen, A. L., Lee, S. Miller, S. K., Witte, J. C. (2011). Gravity and Rossby wave signatures in the tropical troposphere and lower stratosphere based on Southern Hemisphere Additional Ozonesondes (SHADOZ), 1998–2007, *J. Geophys. Res.*, 116, D05302, doi:10.1029/2009JD013429.

Thompson, A. M., Miller, S. K., Tilmes, S., Kollonige, D. W., Witte, J. C., et al. (2012). Southern Hemisphere Additional Ozonesondes (SHADOZ) tropical ozone climatology: Tropospheric and tropical tropopause layer (TTL) profiles with comparisons to OMI based ozone products. *J. Geophys. Res.*, 117, D23301, doi: 10.1029/2010JD016911.

Thompson, A. M., Witte, J. C., Sterling, C., Jordan, A., Johnson, B. J., Oltmans, S. J., et al. (2017). First reprocessing of Southern Hemisphere Additional Ozonesondes (SHADOZ) ozone profiles (1998–2016): 2. Comparisons with satellites and ground-based instruments, *J. Geophys. Res. Atmos.*, 122, 13,000–13,025, <https://doi.org/10.1002/2017JD027406>.

Wargan, K., Orbe, C., Pawson, S., Ziemke, J. R., Oman, L. D., Olsen, M. A., et al. (2018). Recent decline in extratropical lower stratospheric ozone attributed to circulation changes, *Geophys. Res. Lett.*, 45, 5166–5176, <https://doi.org/10.1029/2018GL077406>.

Witte, J. C., Thompson, A. M., Smit, H. G. J., Fujiwara, M., Posny, F., et al. (2017). First reprocessing of Southern Hemisphere ADditional Ozonesondes (SHADOZ) profile records (1998-2015): 1. Methodology and evaluation, *J. Geophys. Res. Atmos.*, 122, doi:10.1002/2016JD026403.

Witte, J. C., Thompson, A. M., Smit, H. G. J., Fujiwara, M., Johnson, B. J., et al. (2018).
First reprocessing of Southern Hemisphere ADDitional Ozonesondes (SHADOZ) profile records
(1998-2016): 3. Methodology and evaluation, *J. Geophys. Res. Atmos.*, 123,
doi:10.1002/2017JD027791.

Zhang, Y. Cooper, O. R., Gaudel, A., Thompson, A. M., Nédelec, P., Ogino, S.-Y., West,
J. J. (2016). Equatorward redistribution of emissions dominates the 1980 to 2010 tropospheric
ozone change, *Nature-Geoscience*, doi: 10.1038/NGEO282.

Ziemke, J. R., Oman, L. D., Strode, S. A., Douglass, A. R., Olsen, M. A., et al. (2019).
Trends in Global Tropospheric Ozone Inferred from a Composite Record of
TOMS/OMI/MLS/OMPS Satellite Measurements and the MERRA-2 GMI Simulation, *Atmos.*
Chem. Phys. 19, 3257–3269, doi: <https://doi.org/10.5194/acp-19-3257-2019>.

Table 1. SHADOZ site metadata including number of profiles and index terms used in MLR ozone calculations. Monthly MLR partial column ozone linear trends are shown, with significant trends in bold. Significant annual trends occur only at SC-Para (all levels) and Nat-Asc (10 to 15 km). Note: As an independent check of the ozone profile trends (Figure 4), partial column ozone for each layer was calculated and subsequently input into the MLR to derive these statistics.

Site	Lat, Lon (°)	N	MLR Terms	Jan	Feb	Mar	Apr	May	Jun	Jul	Aug	Sep	Oct	Nov	Dec	Ann
SC-Para	5.8, -55.21/ -0.92, -89.62	1190	ENSO+QBO													
5-10 km				-2.1	6.4	12.3	9.7	4.3	4.3	7.1	7.0	5.2	4.8	2.6	-2.0	5.0
10-15 km				-7.8	-4.1	12.6	17.9	1.1	-4.3	4.3	12.4	11.2	11.0	11.5	2.9	5.7
15-20 km				1.2	3.3	2.5	0.1	-3.3	-6.6	-8.1	-7.7	-5.9	-4.8	-4.6	-2.6	-3.0
Nat-Asc	-5.42, -35.38/ -7.58, 14.24	1363	ENSO+QBO													
5-10 km				-1.1	0.1	1.0	1.1	2.3	4.0	3.5	0.9	-0.7	-0.3	0.1	-0.7	0.8
10-15 km				7.9	7.7	3.3	1.5	2.8	3.4	4.2	5.5	4.3	1.5	0.3	3.3	3.8
15-20 km				8.4	11.1	6.3	2.3	1.2	-2.1	-5.6	-5.9	-3.2	-1.6	-1.5	1.7	0.9
Nairobi	-1.27, 36.8	905	ENSO+QBO													
5-10 km				4.3	12.6	13.7	4.8	-3.3	-3.8	-0.4	1.5	1.2	1.1	0.7	0.4	2.7
10-15 km				-1.1	4.4	6.9	4.4	1.3	2.2	3.2	-1.9	-6.1	-5.2	-2.6	-1.9	0.3
15-20 km				4.5	10.0	11.8	6.5	-0.8	-5.2	-5.9	-4.3	-1.1	1.6	1.9	1.7	1.7
KL-Java	2.73, 101.27/ -7.5, 112.6	770	ENSO+QBO +DMI													
5-10 km				-3.0	9.5	14.0	4.4	-1.1	1.8	3.2	-1.5	-1.0	3.7	2.1	-4.7	2.3
10-15 km				-6.2	3.9	12.2	11.7	6.9	2.4	-0.5	-1.3	0.5	0.9	-3.2	-8.2	1.6
15-20 km				-2.1	1.2	1.0	1.2	2.2	-0.6	-5.6	-7.4	-4.7	-2.7	-4.0	-4.9	-2.2
Samoa	-14.23, -170.56	752	ENSO+QBO													
5-10 km				3.7	6.4	6.4	-1.5	-5.6	-1.1	4.1	0.9	-4.7	-4.3	0.4	3.0	0.6
10-15 km				12.4	19.6	16.2	11.3	3.1	-3.5	-5.3	0.1	4.4	-0.5	-5.9	-1.4	4.2
15-20 km				0.3	6.8	3.8	-4.2	-5.3	-1.7	-1.3	-2.3	-0.7	0.8	-1.8	-4.0	-0.8

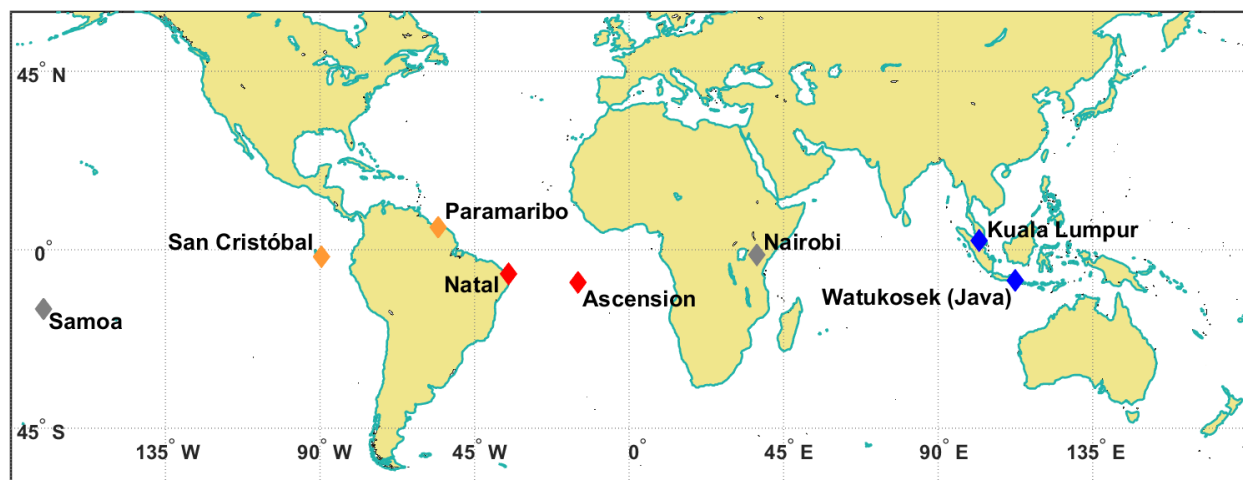


Figure 1. Map of SHADOZ stations used in this study. Stations whose combined records are examined are colored orange (San Cristóbal and Paramaribo), red (Natal and Ascension), and blue (Watukosek and Kuala Lumpur). Samoa and Nairobi records are studied individually and colored grey. Sample numbers appear in Table 1.

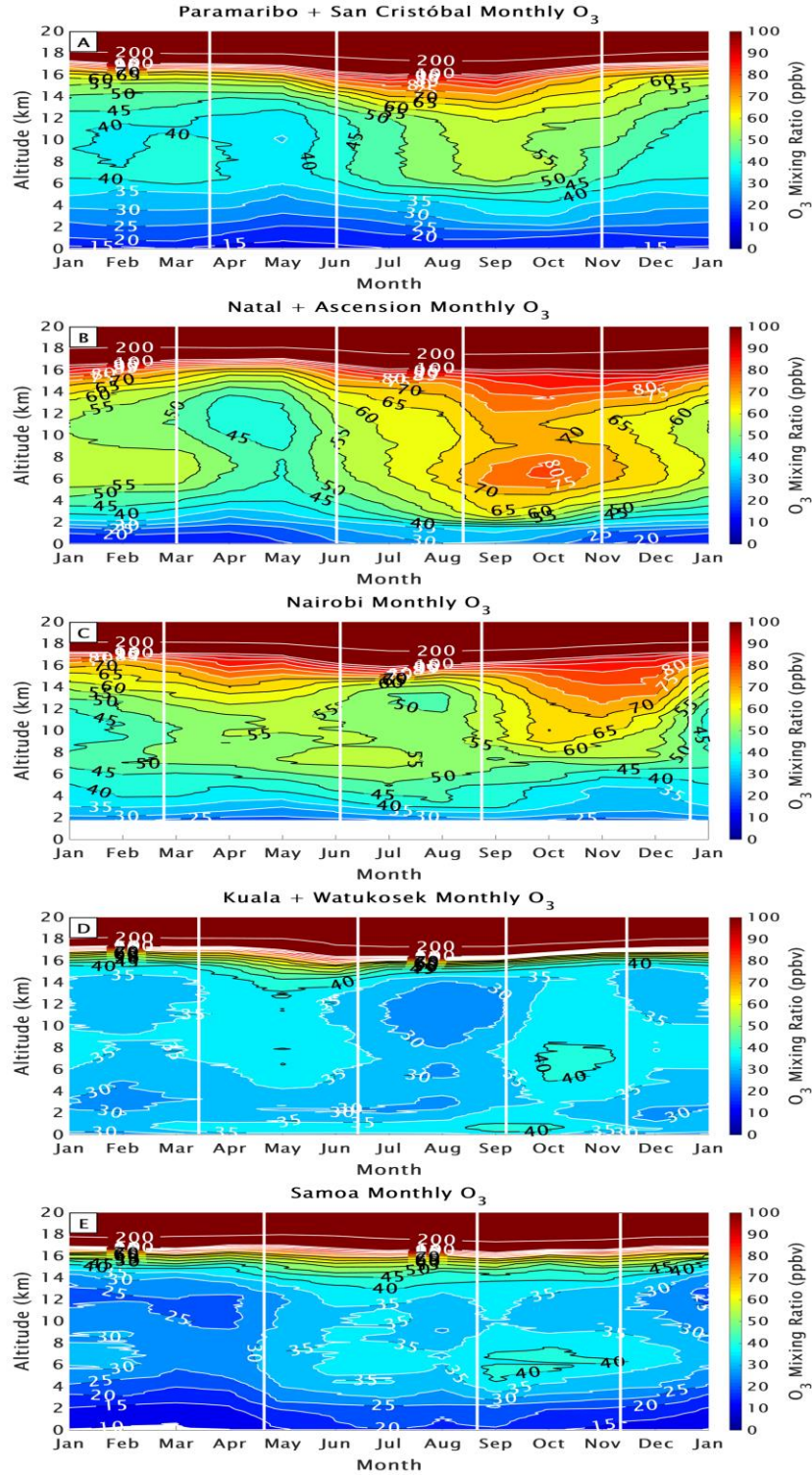


Figure 2. Monthly averaged ozone mixing ratios from the surface to 20 km altitude for the five sites: two individual and three combinations. White dashed lines indicate transition periods marked by > 5 ppbv changes to the climatological FT and LMS ozone distributions (Figure S3).

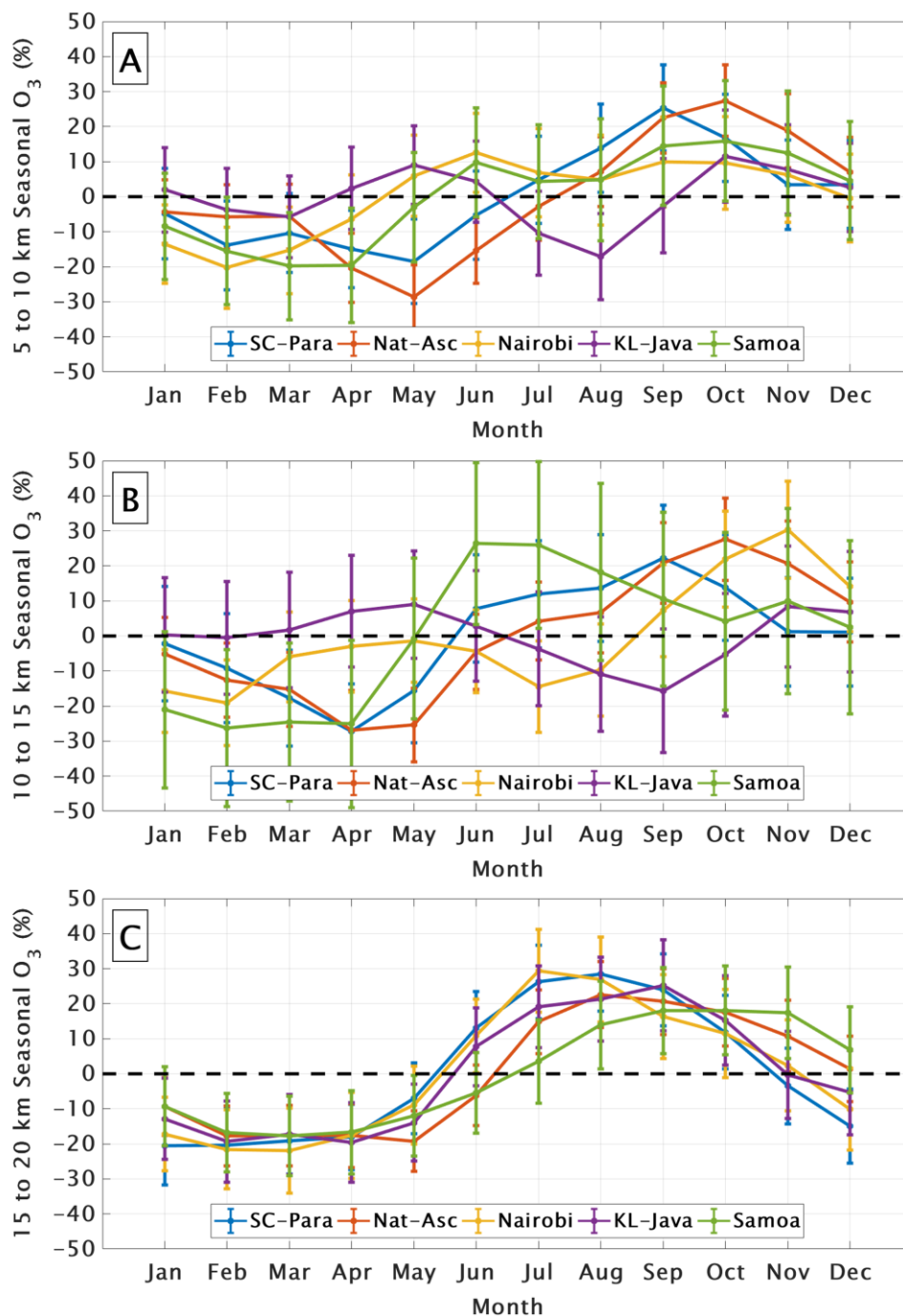


Figure 3. Seasonal variability in ozone in the FT (a and b), and LMS (c) expressed as percent anomaly, based on ozone mixing ratio deviation from the annual mean at the two individual and three combination sites.

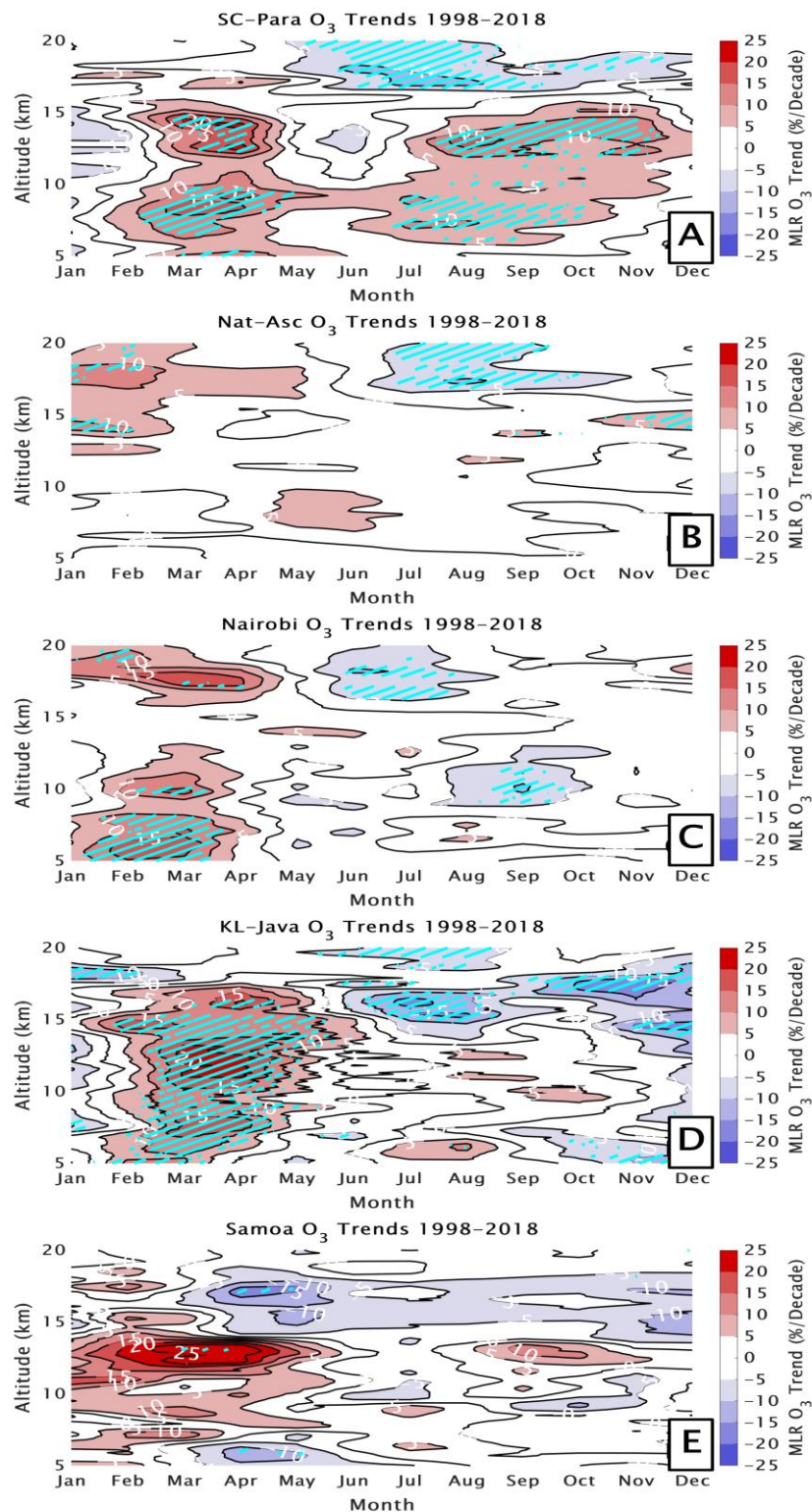
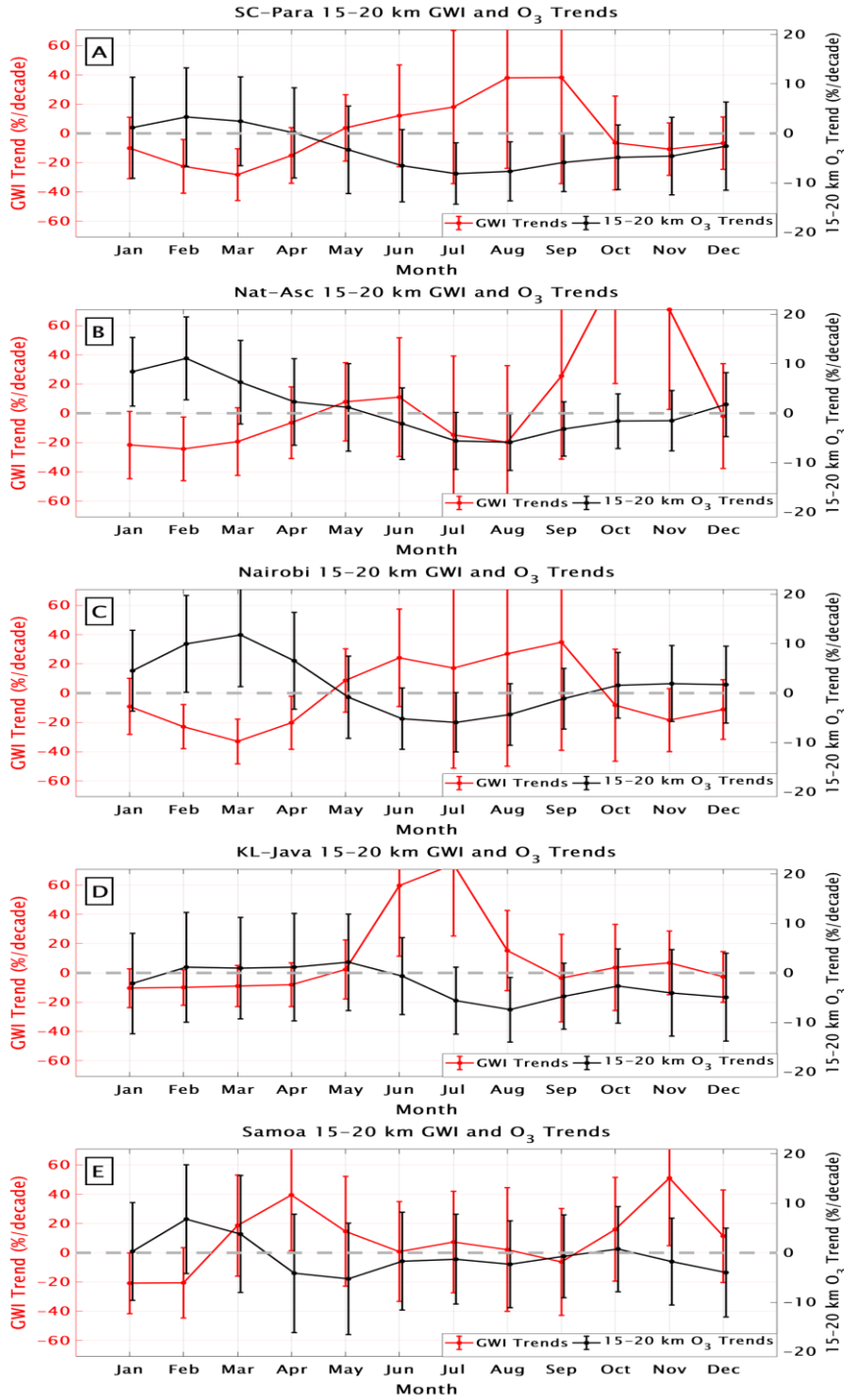


Figure 4. Monthly MLR ozone linear trends from 5 to 20 km in percent per decade for the two individual and three combination sites. Positive trends are shown in red and negative trends are shown in blue. Trends that are significant with 95% confidence are shown with cyan hatching.

387



388

389

390 Figure 5. Monthly MLR gravity wave index (GWI) linear trends (red) and 15 to 20 km (LMS)
 391 partial column ozone linear trends (black) for the two individual and three combination sites. The
 392 dots represent the values and the error bars indicate the 95% confidence intervals. Values for the
 393 black lines can be found in Table 1.

Figure 1.

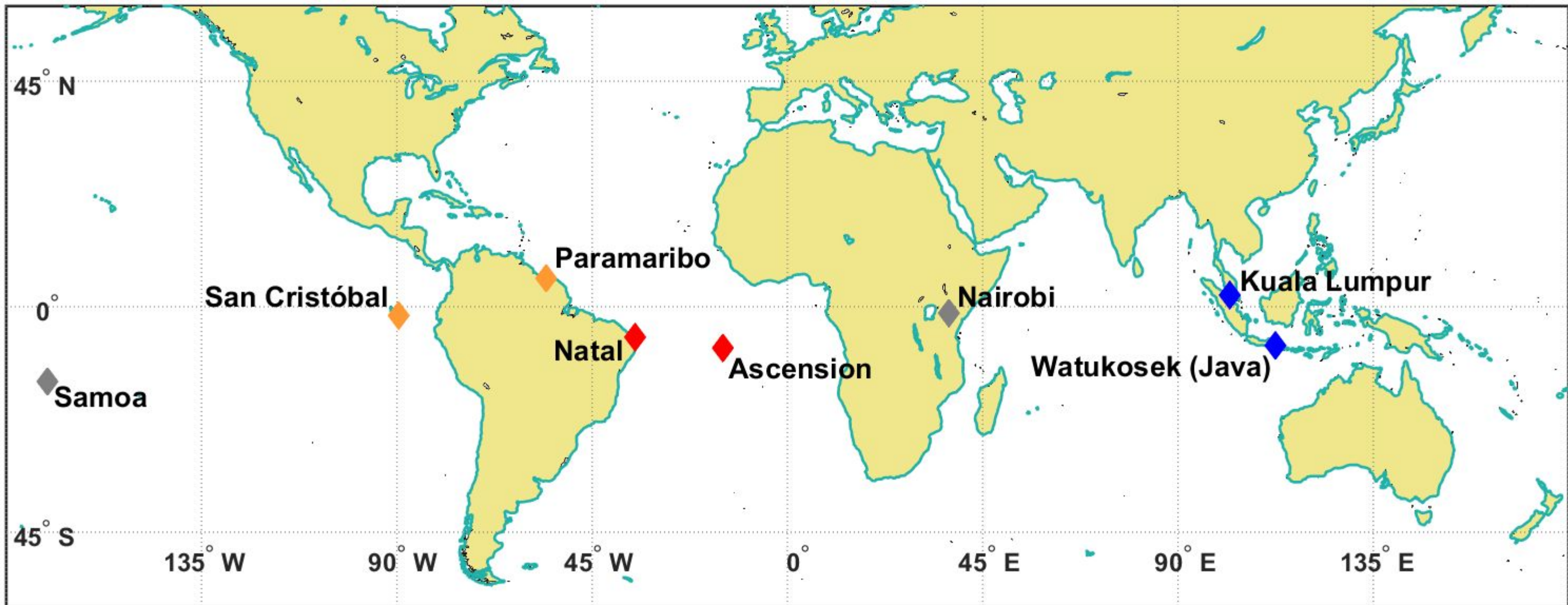
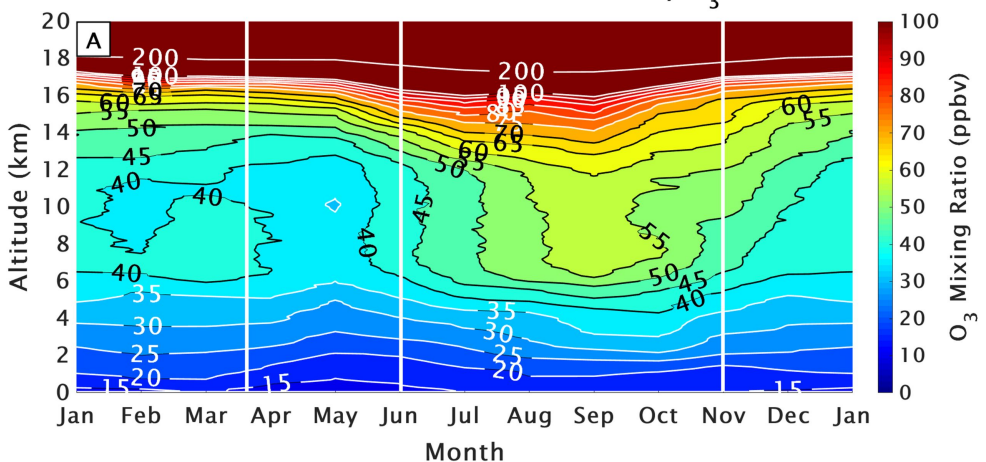
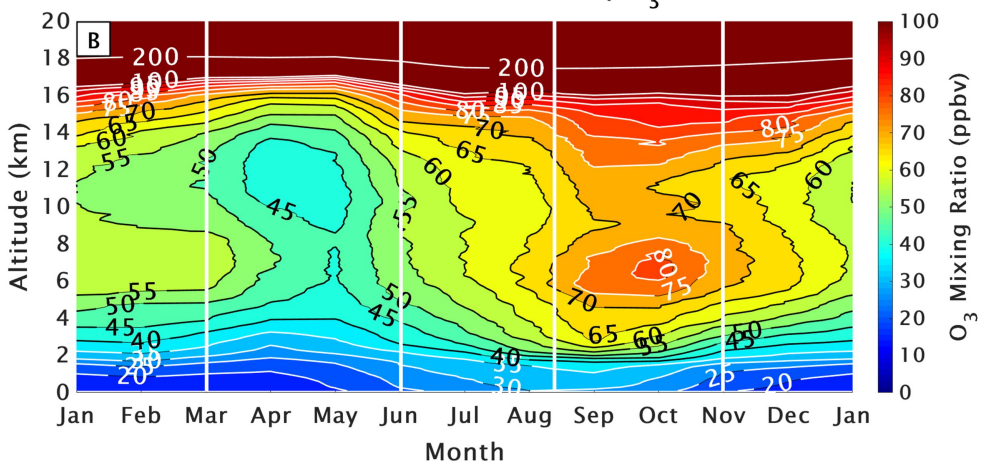


Figure 2.

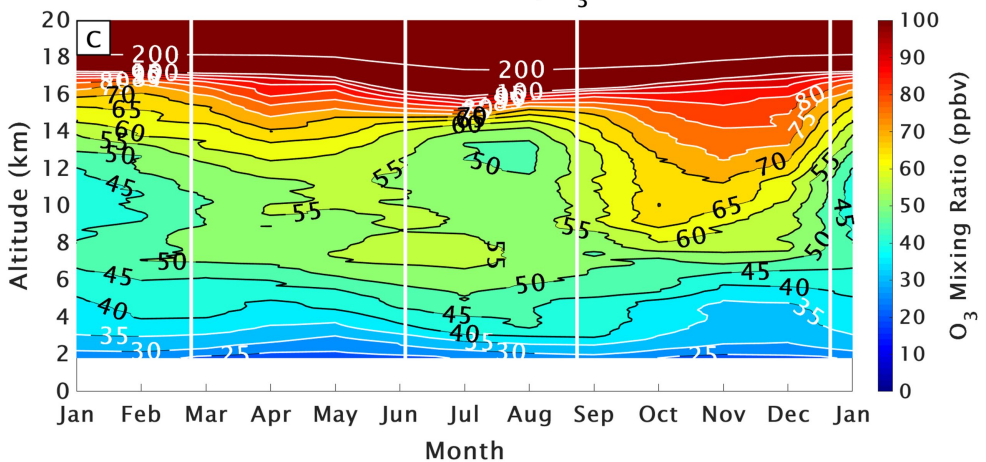
Paramaribo + San Cristóbal Monthly O_3



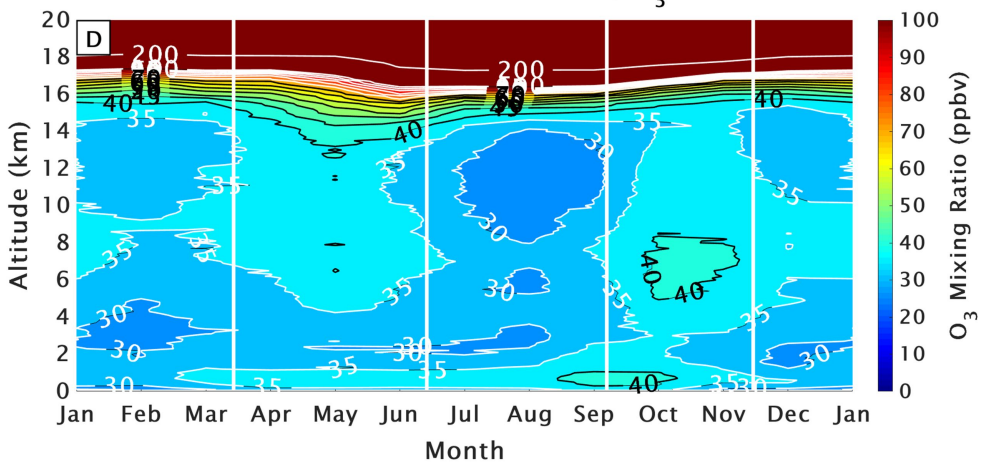
Natal + Ascension Monthly O_3



Nairobi Monthly O_3



Kuala + Watukosek Monthly O_3



Samoa Monthly O_3

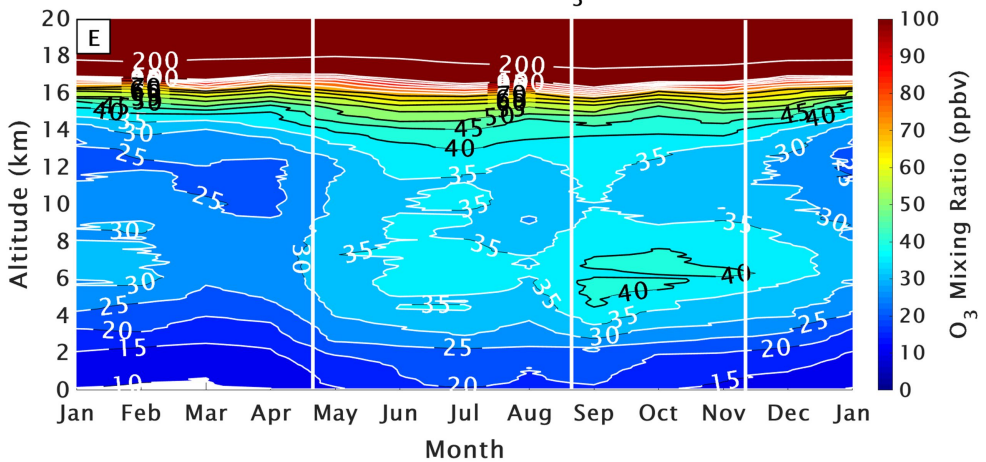


Figure 3.

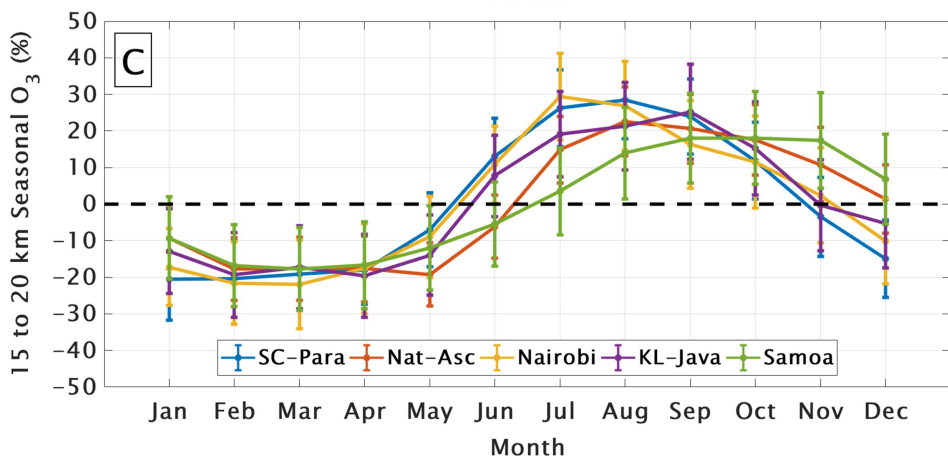
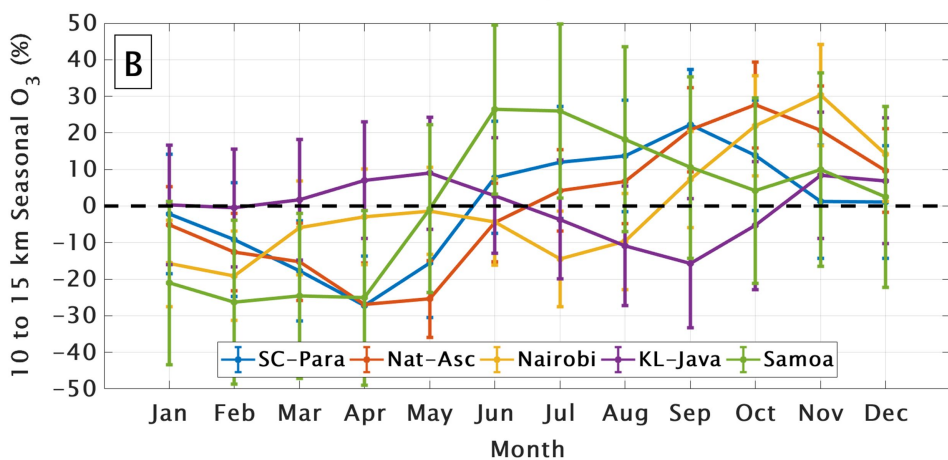
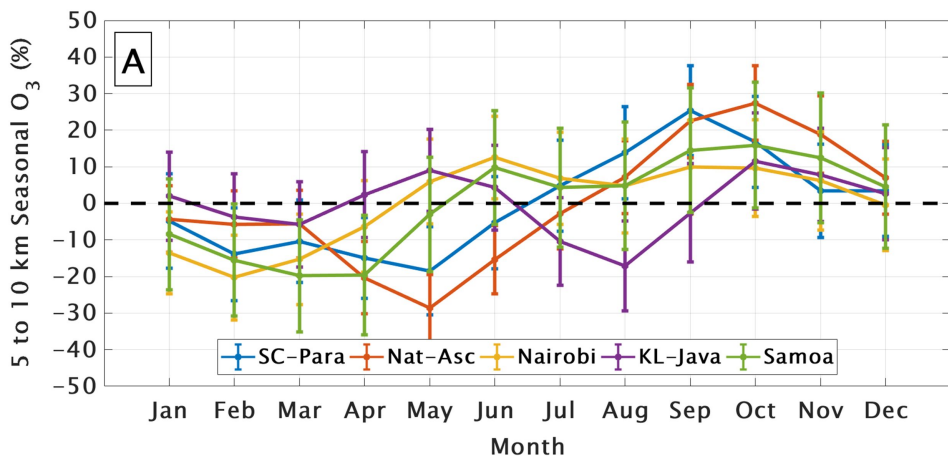
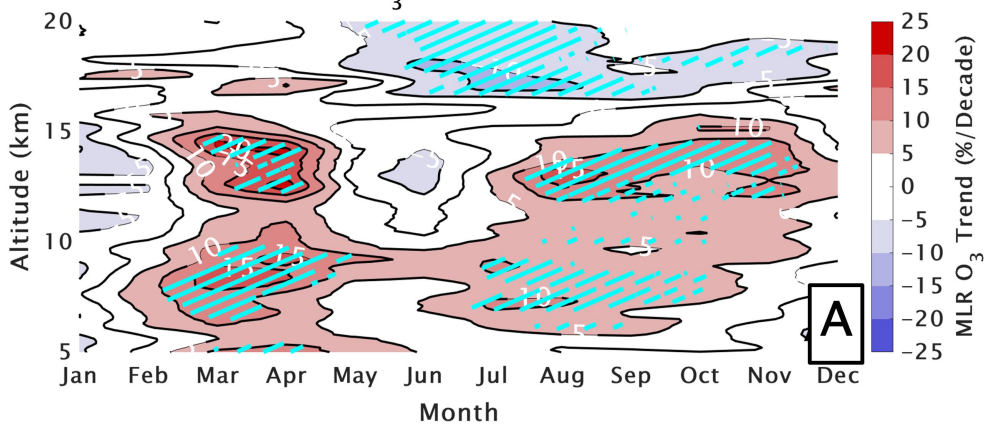
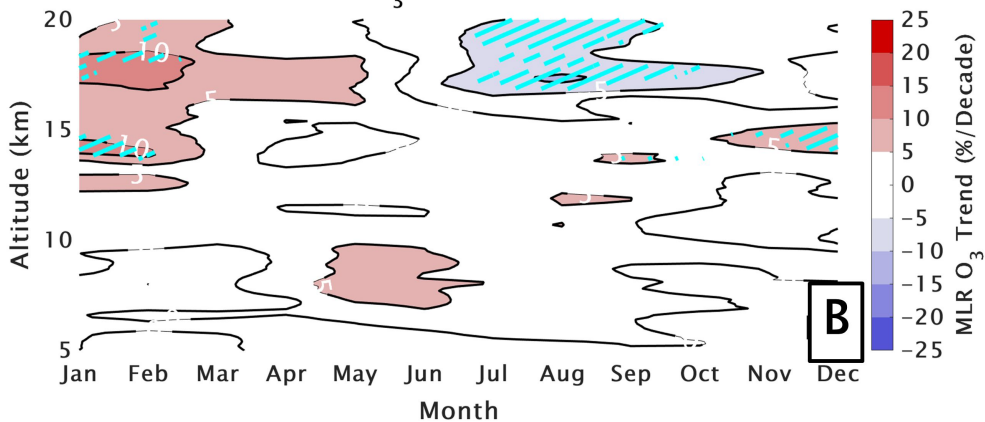


Figure 4.

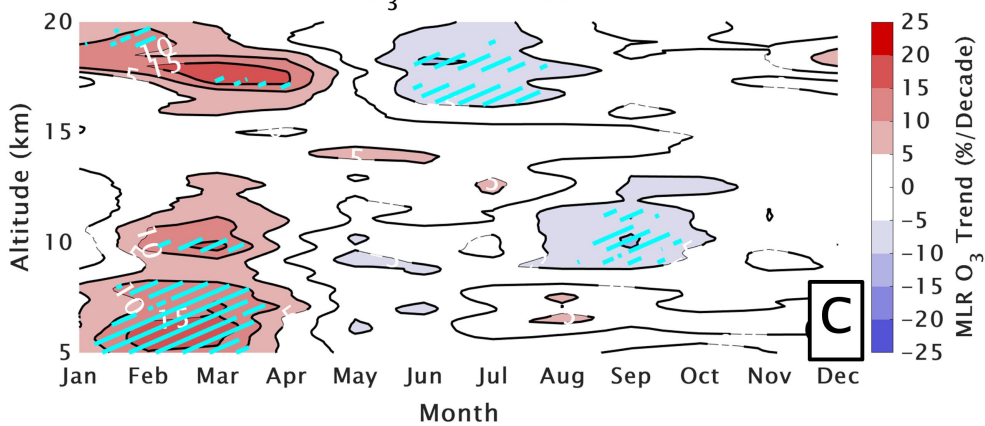
SC-Para O₃ Trends 1998–2018



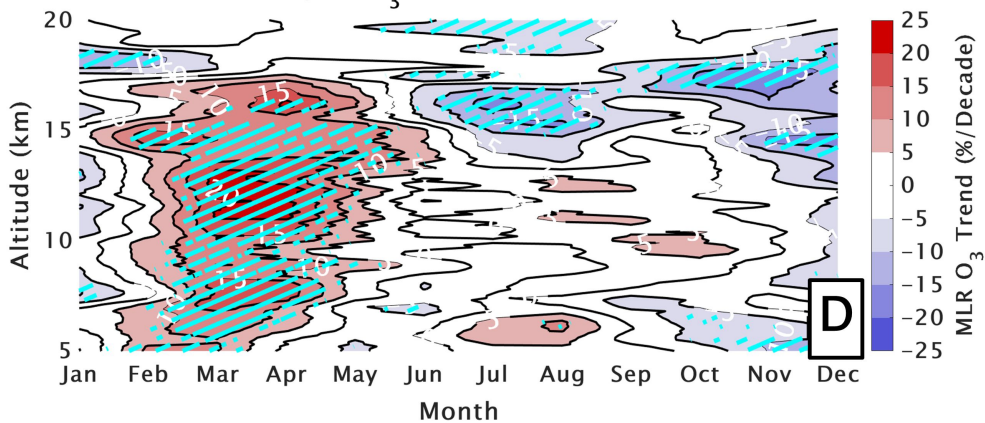
Nat-Asc O₃ Trends 1998–2018



Nairobi O₃ Trends 1998–2018



KL-Java O₃ Trends 1998–2018



Samoa O₃ Trends 1998–2018

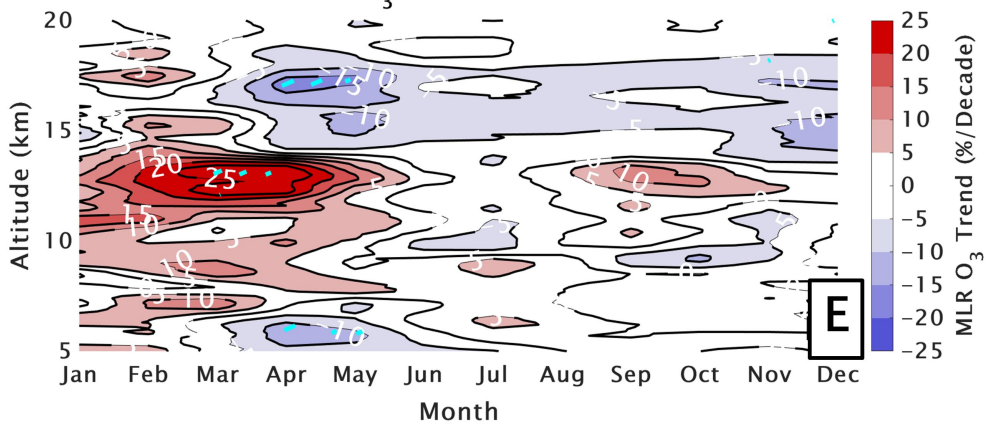
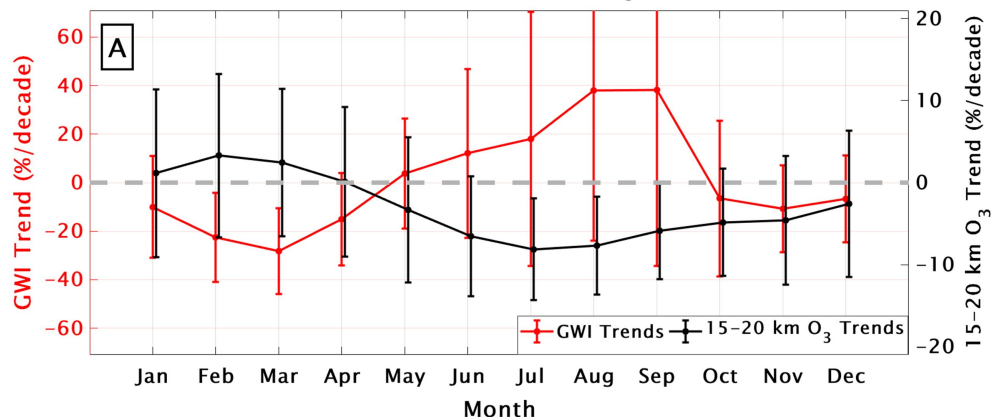
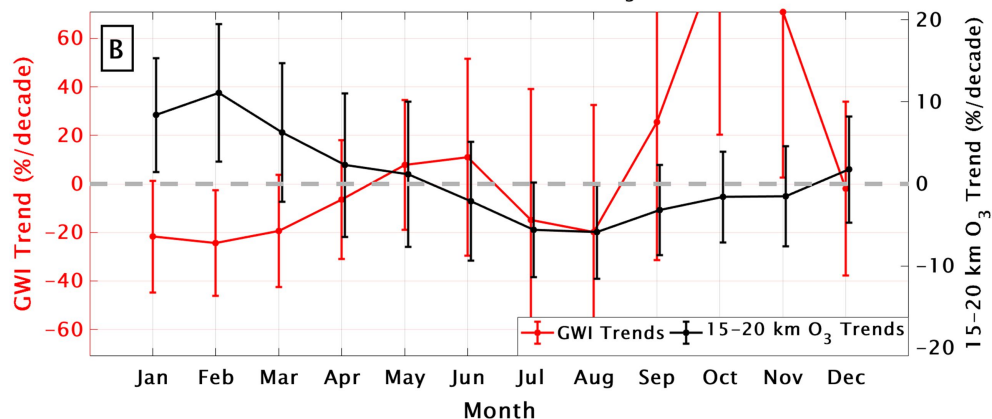


Figure 5.

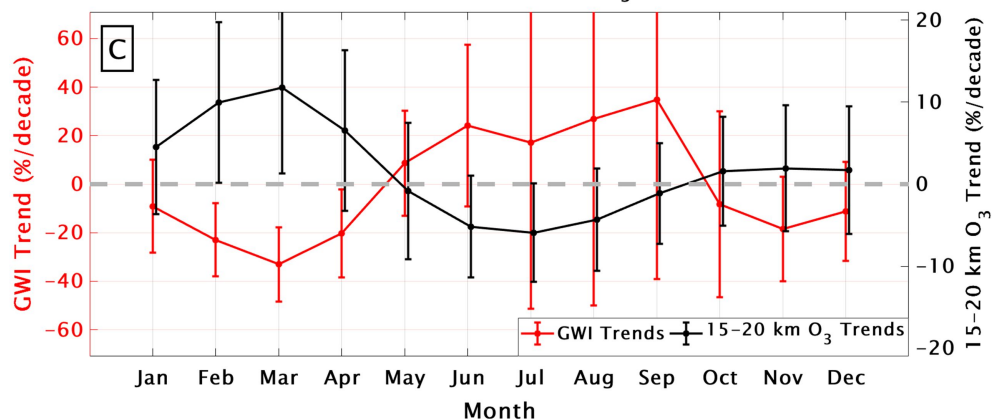
SC-Para 15-20 km GWI and O₃ Trends



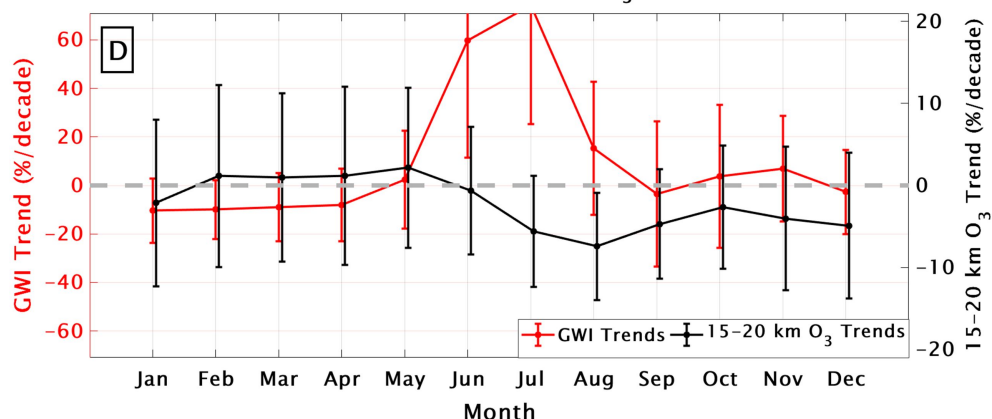
Nat-Asc 15-20 km GWI and O₃ Trends



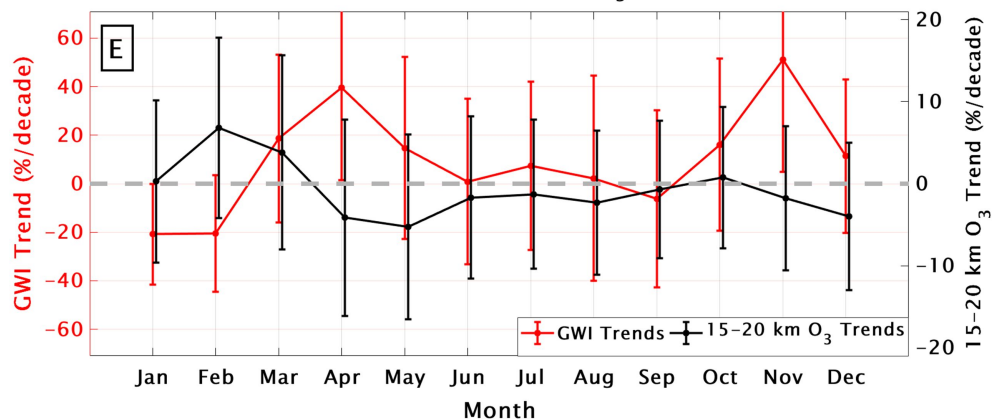
Nairobi 15-20 km GWI and O₃ Trends



KL-Java 15-20 km GWI and O₃ Trends



Samoa 15-20 km GWI and O₃ Trends



**The Role of Convection in Tropical Ozone Trends (1998-2018)
Based on SHADOZ Profiles**

**Anne M. Thompson^{1*}, Ryan M. Stauffer^{1,2}, Jacquelyn C. Witte³, Debra E.
Kollonige^{1,4}, Krzysztof Wargan^{1,4}, Jerry R. Ziemke^{1,5}**

¹ NASA/Goddard Space Flight Center (GSFC), Greenbelt, MD, USA

²Earth System Science Interdisciplinary Center, University of Maryland, College Park,
MD, USA

³National Center for Atmospheric Research Earth Observations Laboratory, Boulder, CO,
USA

⁴Science Systems and Applications, Inc., Lanham, MD, USA

⁵Morgan State University, Baltimore, Maryland, USA

*Corresponding author: Anne M. Thompson (anne.m.thompson@nasa.gov)

Contents of this file

Figures S1 to S6

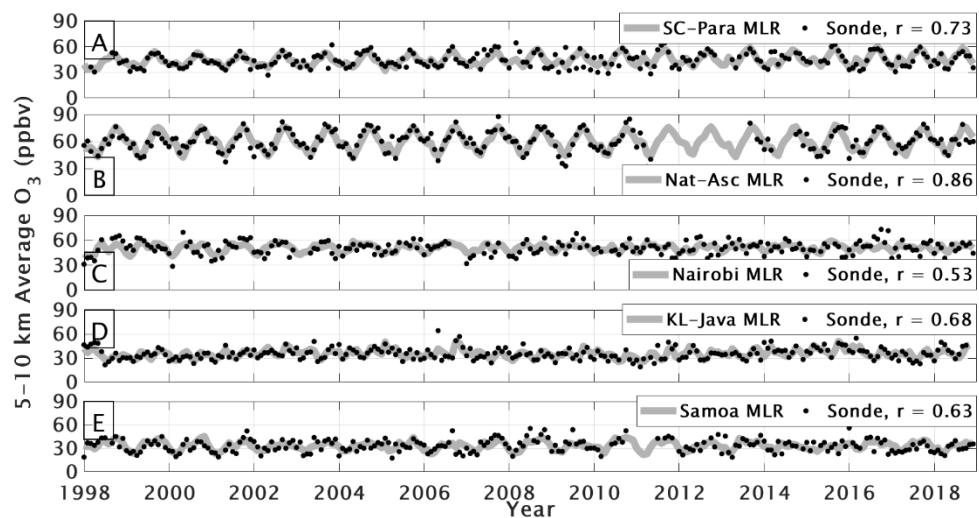


Figure S1. Monthly averaged MLR (grey lines) and ozonesonde (black dots) ozone (O_3) mixing ratios for the two individual and three combination sites in the 5 to 10 km layer. Correlations between MLR and ozonesonde data are shown in each legend.

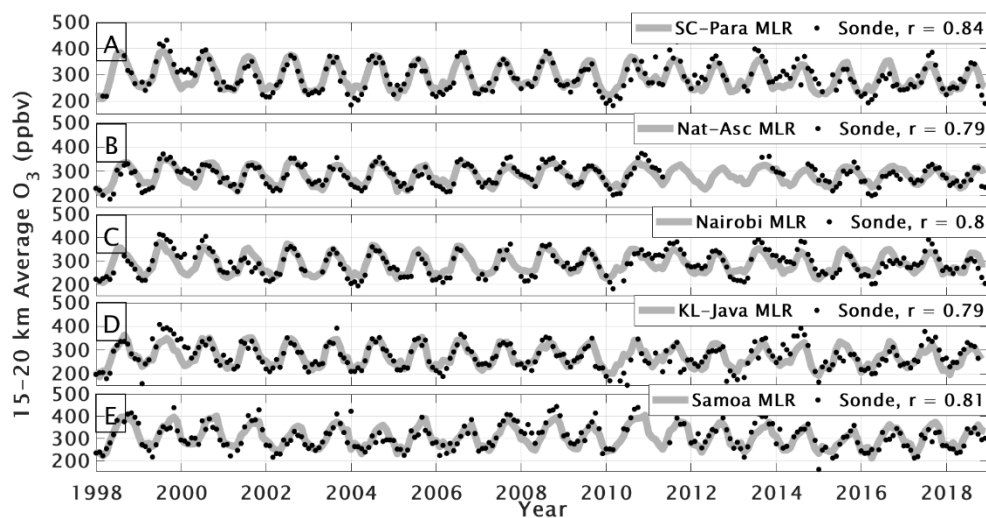


Figure S2. Monthly averaged MLR (grey lines) and ozonesonde (black dots) ozone (O_3) mixing ratios for the two individual and three combination sites in the 15 to 20 km (LMS) layer. Correlations between MLR and ozonesonde data are shown in each legend.

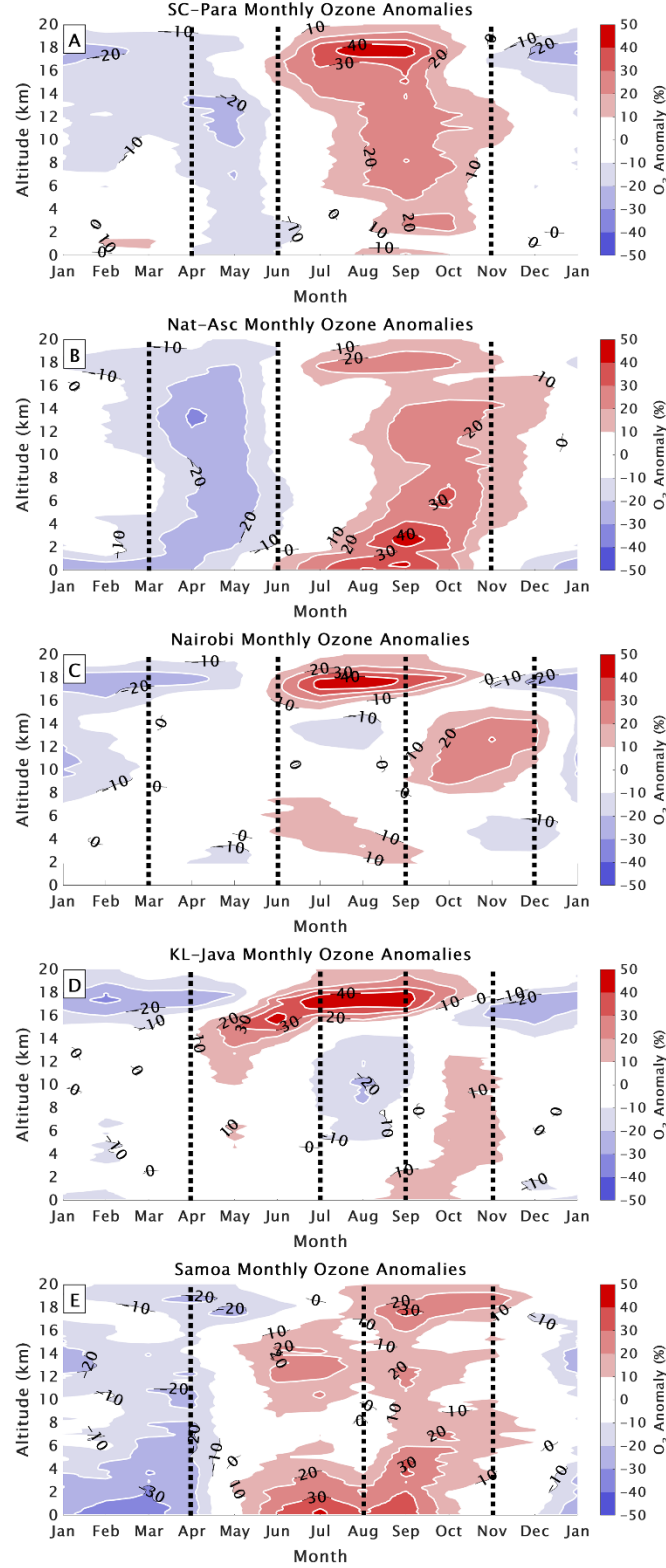


Figure S3. Monthly averaged ozone (O_3) mixing ratio anomalies in percent from the annual mean from the surface to 20 km altitude for the two individual and three combination sites. Black dashed lines (same as the white dashed lines in Figure 2) indicate transition periods marked by large changes to the climatological FT and LMS O_3 amounts.

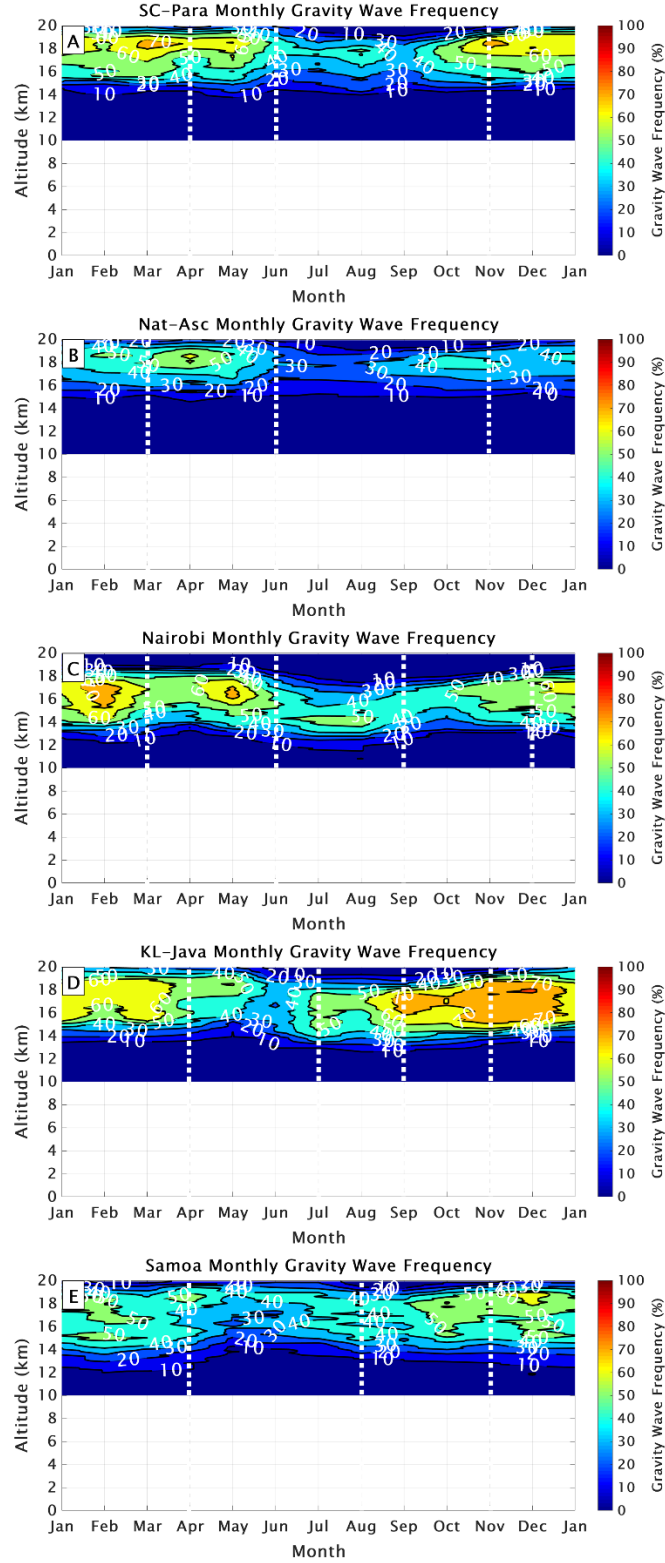


Figure S4. Monthly averaged gravity wave frequency (GWF) in percent from 10 to 20 km altitude corresponding to the profiles in Figure 2 for the two individual and three combination sites. White dashed lines are set by the ozone (O_3) mixing ratio gradients as shown in Figures 2 and S3.

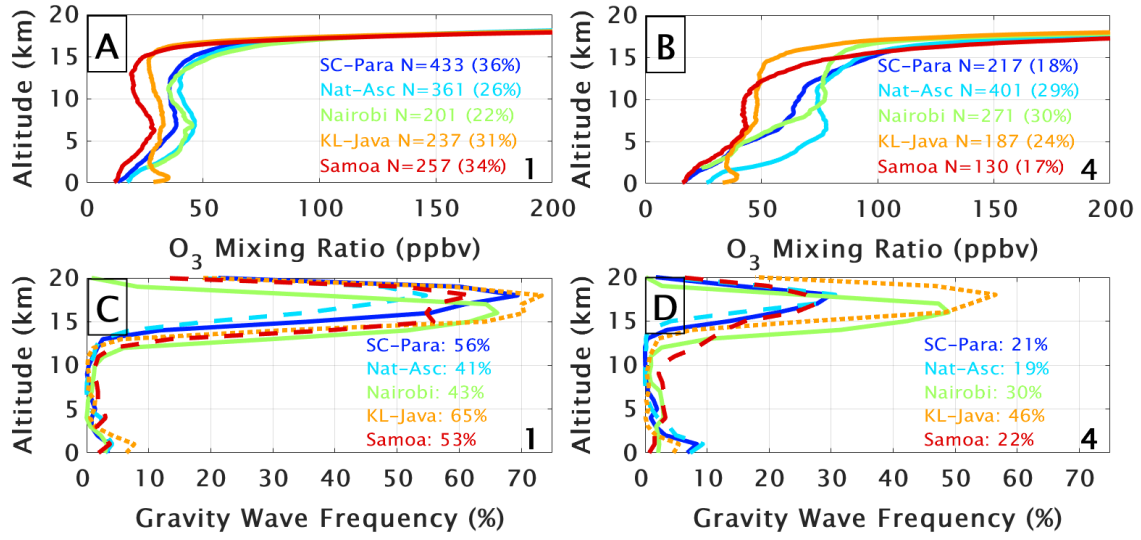


Figure S5. (a, b): SOM cluster ozone means for the two individual and three combination sites. The number and percentage of profiles contributing to each of four clusters (two not shown) appear in each frame. (c, d): Gravity wave frequency (GWF in text) as a function of altitude corresponding to SOM clusters 1 and 4. Average GWF from 15 to 20 km (LMS) for each site is shown in the frames.

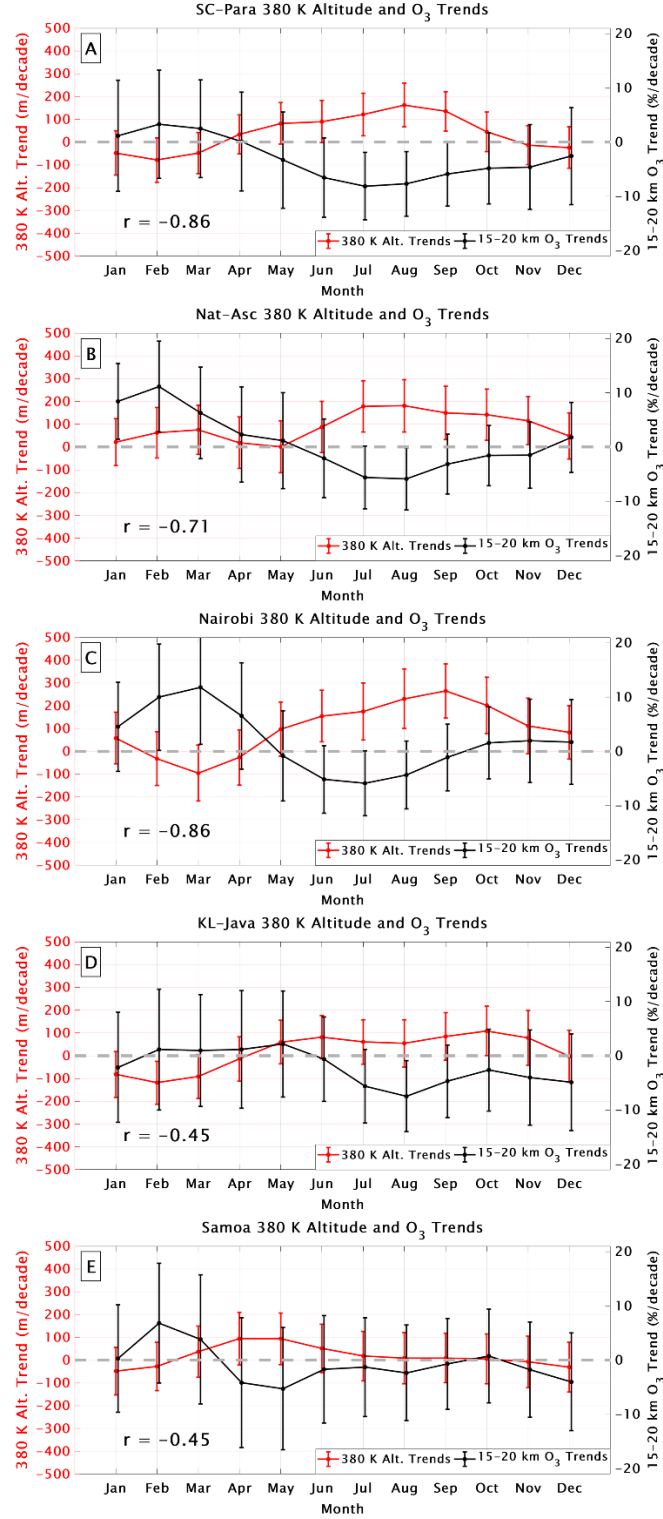


Figure S6. Monthly MLR linear trends in the altitude of the 380 K potential temperature level (red) and 15 to 20 km (LMS) partial column ozone (O_3) linear trends (black) for the five SHADOZ sites. The dots represent the values and the error bars indicate the 95% confidence intervals. Correlations between the altitude of the 380 K potential temperature surface, our proxy for the tropopause, and LMS O_3 trends are shown on each panel.